PTOL - Point Takeoff Landing (Project A)

Research Project Report, Course #085851

Mike Manasherov

Advisers: Prof. Moshe Idan, Prof. Gil Iosilevslii

September 2023

Abstract

The objective of this project is to examine the longitudinal dynamics of a new configuration of an aircraft for point takeoff and landing without the need for a runway while providing the capability to fly short to mid-ranges at high velocity and efficiently. The discussed aircraft will have the ability to tilt its wing and rotors together to enable low-velocity flight. The aircraft is equipped with wake flaps located downstream of the propellers to control low-velocity flights. This part of the research aims to develop a dynamic model of the proposed configuration that will be the basis for a control system design of the aircraft addressed in the following stages of the project. An analytical aerodynamic model is constructed for this work. This initial study addresses mainly the trim flight of the aircraft while analyzing the effect of system parameters on the trim variables.

List of Symbols

Symbols

α	Angle of attack
δ	Control surface deflection angle
γ	Trajectory angle
ω	Angular velocity
ρ	Propeller radius
θ	Pitch angle
c	Reference wing chord
g	Gravity acceleration
I	Moment of inertia around the Y axis
i	Incidence angle
l	Element center of gravity ahead of the hinge

m Element mass

R Reaction forces around the hinge

S Reference wing area

u Velocity in the X axis

V Total velocity, $V = \sqrt{u^2 + w^2}$

w Velocity in the Z axis

X Element total aerodynamic force in the X axis

Z Element total aerodynamic force in the Z axis

Subscripts

b Body related variables

p Propeller related variables

w Wing related variables

x X axis related variables

z Z axis related variables

1 Introduction

Rapid short to mid-range transportation has become a challenge in recent decades. The goal is to develop an aircraft capable of covering these ranges in a short time while taking off and landing without the need for a runway. Using multi-rotors for this mission will lead to low flight speed and short range while using fixed-wing configurations will require a runway. To solve this conflict, we propose combining the advantages of both configurations to yield an aircraft capable of flying short to mid-ranges at high velocity and also landing at low velocity without the need for a runway.

The suggested configuration is an aircraft flying as a standard fixed-wing aerial vehicle at high velocity. To slow down, and mainly to fly at speeds that are below the stall speed of the aircraft, the wings will tilt upwards also rotating the two propeller motors installed on the leading edge of the wings. This will generate a vertical thrust component to balance the weight of the aircraft. In addition, each wing will have a wake-flap located in the prop-wash of the rotor for control during low-velocity flight. This configuration will be used mainly for takeoff and landing.

This project will review the physical and aerodynamic models of the aircraft in the longitudinal plane. Additionally, reviewing the ability to trim at various flight conditions, the effect of some parameters on the dynamics and trimming point will be addressed.

2 Aircraft Configuration and Parameters

The aircraft configuration and the various axis systems used in this study are described in Fig. 1. The wing is attached to the body by a hinge enabling it to rotate around the Y axis. An actuator that is generating moment (denoted by M_{act}) is attached to the hinge and will be used for control. Variable-pitch propeller motors are installed on each wing. They generate the thrust required for the various phases of the flight. Wake flaps, the deflection angle of which are denoted by δ_f, are placed down the stream of the propellers. Affected by the prop-wash, those flaps will be used for control mainly in the take-off and landing phases of the flight. The tail is equipped with an elevator, the deflection angle of which is denoted by δ_e.

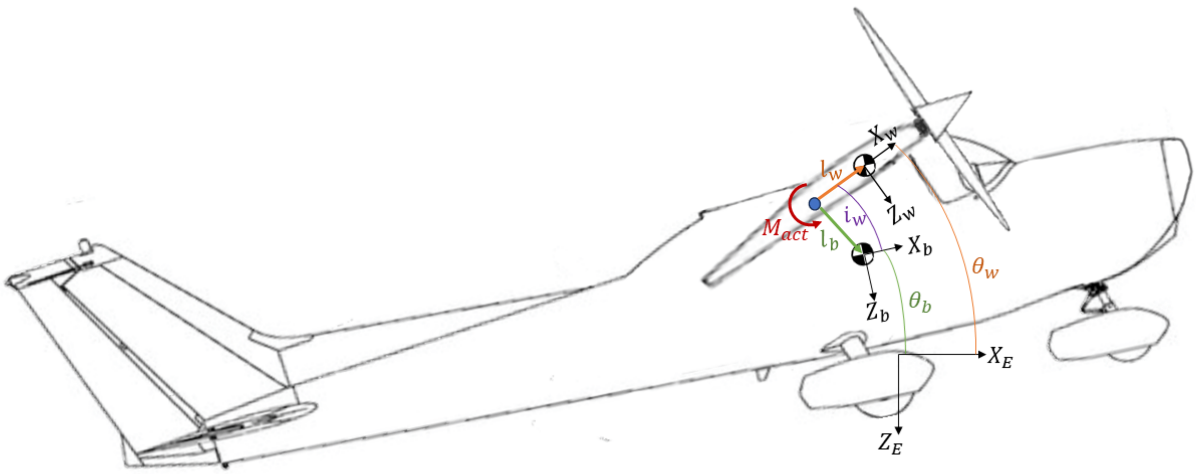

Figure 1: Aircraft Configuration and Axis Systems.

The preliminary system parameters assumed as a basis for this research are summarized in Table 1. These values will, most likely, change according to future needs as the aircraft configuration becomes known. Additionally, the effects of these parameters on the aircraft dynamics can be checked by altering them in the analysis. Similarly, control limits have been assumed as presented in Table 2.

Table 1: Aircraft parameters.

Parameter	**Symbol**	**Value**
Body mass	m_b	450 [kg]
Wing mass	m_w	150 [kg]
Body moment of inertia	I_b	2100 [kg m^2]
Wing moment of inertia	I_w	300 [kg m^2]
Wing surface	S	15 [m^2]
Wing chord	c	1.5 [m]
Propeller radius	ρ	1.2 [m]

Table 2: Control limits.

Control	Symbol	Limit
Rotor rotation speed	ω_p	[1700,2000] [RPM]
Wing tilt angle	i_w	$[-10°, 110°]$
Elevator deflection angle	δ_e	$[-25°, 25°]$
Flaps deflection angle	δ_f	$[-60°, 60°]$
Propeller pitch angle	δ_p	$[10°, 20°]$

3 Dynamic Model

The dynamic model of the proposed configuration assumes that the wing is attached to the aircraft's body with a hinge, resulting in reaction forces in the X and Z directions. At the hinge, an actuator is used to generate a moment M_{act} around the Y axis acting in opposite directions on the wing and to the body of the aircraft.

Using force and moment equations in the longitudinal plane of the inertial coordinate system, the dynamics of the aircraft body are expressed as

$$m_b(\ddot{x} - \ddot{\theta}_b l_b \sin\theta_b - \dot{\theta}_b^2 l_b \cos\theta_b) = X_b + R_x, \tag{1a}$$
$$m_b(\ddot{z} - \ddot{\theta}_b l_b \cos\theta_b + \dot{\theta}_b^2 l_b \sin\theta_b) = m_b g + Z_b + R_z, \tag{1b}$$
$$I_b\ddot{\theta}_b = M_b + M_{act} + (X_b + R_x) l_b \sin\theta_b + (Z_b + R_z) l_b \cos\theta_b. \tag{1c}$$

Here, (1a) is the force equation in the X direction, (1b) is the force equation in the Z direction, and (1c) is the moment equation around the Y-axis.

Similarly, the equations of motion for the wings are

$$m_w(\ddot{x} - \ddot{\theta}_w l_w \sin\theta_w - \dot{\theta}_w^2 l_w \cos\theta_w) = X_w - R_x, \tag{2a}$$
$$m_w(\ddot{z} - \ddot{\theta}_w l_w \cos\theta_w + \dot{\theta}_w^2 l_w \sin\theta_w) = m_w g + Z_w - R_z, \tag{2b}$$
$$I_w\ddot{\theta}_w = M_w - M_{act} + (X_w - R_x) l_w \sin\theta_w + (Z_w - R_z) l_w \cos\theta_w. \tag{2c}$$

Combining the X-axis force equations (1a) and (2a), the Z-axis equations(1b) and (2b) yields

$$\begin{aligned}(m_b + m_w)\cdot\ddot{x} - m_b l_b \sin\theta_b\cdot\ddot{\theta}_b - m_w l_w \sin\theta_w\cdot\ddot{\theta}_w \\ = m_b l_b \cos\theta_b\cdot\dot{\theta}_b^2 + m_w l_w \cos\theta_w\cdot\dot{\theta}_w^2 + X_b + X_w,\end{aligned} \tag{3a}$$
$$\begin{aligned}(m_b + m_w)\cdot\ddot{z} - m_b l_b \cos\theta_b\cdot\ddot{\theta}_b - m_w l_w \cos\theta_w\cdot\ddot{\theta}_w \\ = (m_b + l_b)g - m_b l_b \sin\theta_b\cdot\dot{\theta}_b^2 + m_w l_w \sin\theta_w\cdot\dot{\theta}_w^2 + Z_b + Z_w.\end{aligned} \tag{3b}$$

Using the force equations (1a), (1b), (2a) and (2b) to isolate the reaction forces and substituting them into (1c) and (2c) yields

$$-m_b l_b \sin\theta_b\cdot\ddot{x} - m_b l_b \cos\theta_b\cdot\ddot{z} + (I_b + m_b l_b^2)\cdot\ddot{\theta}_b = -m_b g l_b \cos\theta_b + M_b + M_{act}, \tag{3c}$$
$$-m_w l_w \sin\theta_w\cdot\ddot{x} - m_w l_w \cos\theta_w\cdot\ddot{z} + (I_w + m_w l_w^2)\cdot\ddot{\theta}_w = -m_w g l_w \cos\theta_w + M_w - M_{act}. \tag{3d}$$

Finally, the equations of motion in (3) can be restated in a matrix form as

$$\begin{bmatrix} m_b + m_w & 0 & -m_b l_b \sin\theta_b & -m_w l_w \sin\theta_w \\ 0 & m_b + m_w & -m_b l_b \cos\theta_b & -m_w l_w \cos\theta_w \\ -m_b l_b \sin\theta_b & -m_b l_b \cos\theta_b & I_b + m_b l_b^2 & 0 \\ -m_w l_w \sin\theta_w & -m_w l_w \cos\theta_w & 0 & I_w + m_w l_w^2 \end{bmatrix} \begin{Bmatrix} \ddot{x} \\ \ddot{z} \\ \ddot{\theta}_b \\ \ddot{\theta}_w \end{Bmatrix}$$
$$= \begin{Bmatrix} m_b l_b \cos\theta_b \cdot \dot{\theta}_b^2 + m_w l_w \cos\theta_w \cdot \dot{\theta}_w^2 + X_b + X_w \\ (m_b + m_w) g - m_b l_b \sin\theta_b \cdot \dot{\theta}_b^2 - m_w l_w \sin\theta_w \cdot \dot{\theta}_w^2 + Z_b + Z_w \\ -m_b g l_b \cos\theta_b + M_b + M_{act} \\ -m_w g l_w \cos\theta_w + M_w - M_{act} \end{Bmatrix}. \quad (4)$$

Unsurprisingly, the dynamic model of the system, as given in (4), is nonlinear.

4 Aerodynamic Model

Similar to the equations of motion, the aerodynamic model is constructed of the contributions of the wing and the body separately. For the wing, the aerodynamic model is constructed from the contribution of the part of the wing that is in the prop-wash and the rest of the wing. In the prop-wash, the absolute local angle of attack is smaller and the dynamic pressure is higher as the local stream speed is higher. It is assumed that the stall in each region is independent, but we are more likely to see the region outside the prop-wash stalling first, as the absolute local angle of attack there is higher. At low velocity, the forces and moments are mainly generated by the rotors and the wings, as the dynamic pressure there is high. As the velocity increases, moments generated by the aircraft's tail become more significant, and the aircraft will probably behave similarly to typical fixed-wing aircraft.

5 Trimming

The trim of an aircraft is defined by a set of system states and inputs such that the translational and angular accelerations of the vehicle are zero, i.e.,

$$\ddot{x} = \ddot{z} = \ddot{\theta}_b = \ddot{\theta}_w = 0. \quad (5)$$

The trim variables are obtained by enforcing the conditions in (5) on (4). As the resulting algebraic equations are non-linear, a numeric search will be used to solve them, specifically, the `fsolve` function of MATLAB.

Since trim is computed by solving four algebraic equations, which are functions of eight states and five inputs, the values of all but four of those variables have to be set according to the desired flight conditions, while the remaining four will be determined by solving (5). Initially, as reported in this section, the center of gravity of the body has been placed at the hinge, meaning $l_b = 0$, and the center of gravity of the wing is located at a distance $l_w = 0.6$ [m] relative to the hinge. The possible variations in l_b to ensure trim conditions are examined in the following section.

It has been chosen to trim according to the list of variables defined in Table 3. It should be noted that whether the attitude of the aircraft body, the wing, and the elevator are trimmed or set changes between low and high-velocity flight. At high velocity, the behavior of the aircraft is similar to any typical fixed-wing aircraft, but with the ability to control the moment between the wing and the body. Contrary, trimming the aircraft with the same attitude at low velocity is not possible. In this case, instead of controlling the elevator deflection angle δ_e, where the dynamic pressure is low, wake flaps δ_f located down the stream of the rotors might be a better option as the dynamic pressure there is much higher. Moreover, tilting the wing, by changing i_w will lead to better results than pitching the whole aircraft.

Table 3: Trimmed and set variables.

Symbol	High Velocity	Low Velocity
V	Set	Set
ω_p	Set	Set
γ	Set	Set
i_w	Set	Trimmed
δ_f	Set	Trimmed
θ_b	Trimmed	Set
δ_e	Trimmed	Set
δ_p	Trimmed	Trimmed
M_{act}	Trimmed	Trimmed
$\dot{\theta}_b$	Set	Set
$\dot{i}_w$	Set	Set
$\dot{u}$	Set	Set
$\dot{w}$	Set	Set

5.1 High Velocity Trim

At high-velocity flight, the aircraft should behave like a conventional fixed-wing aircraft. The incidence angle of the wing was set to $i_w = 2°$, and the flaps deflection angle to $\delta_f = 0°$. Running the trim procedure discussed above for level flight, i.e., $\gamma = 0°$, at high velocity it was found that it is possible to trim the aircraft at any velocity higher than 24 [m/s]. At lower velocities, the wing stalls and it is not possible to trim the aircraft, just like any other fixed-wing aircraft. The trim results presented in Fig. 2 resemble those of a statically stable fixed-wing aircraft.

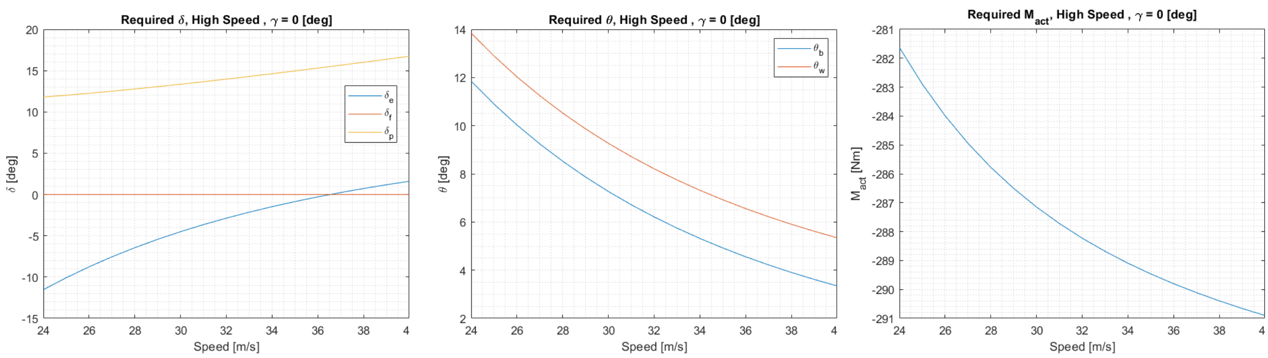

(a) Required δ (b) Required θ (c) Required M_{act}

Figure 2: Trim at high velocity, $\gamma = 0°$.

Figure 2a demonstrates that as the velocity increases, the elevator deflection angle δ_e increases (nose down), and the propeller pitch angle δ_p also increases. The deflection angle of the flaps, δ_f, remains 0, as it is set and not trimmed. Figure 2b shows that the pitch angles decrease as the velocity increases, meaning the angles of attack of the wing and the body decrease, as expected. Also the difference $\theta_w - \theta_b = i_w$ remains the same. Finally, Fig. 2c shows that the required actuator moment M_{act} remains quite the same for all the examined velocities.

Similarly, running the trim procedure for climbing at high-velocity flight gives the expected results shown in Fig. 3. The required propeller pitch δ_f, which is proportionate to the required motor power, is higher, and the body and wing pitch angles θ_b, θ_w are also higher. The elevator deflection angle δ_e is not affected much meaning the aircraft's static stability is quite neutral.

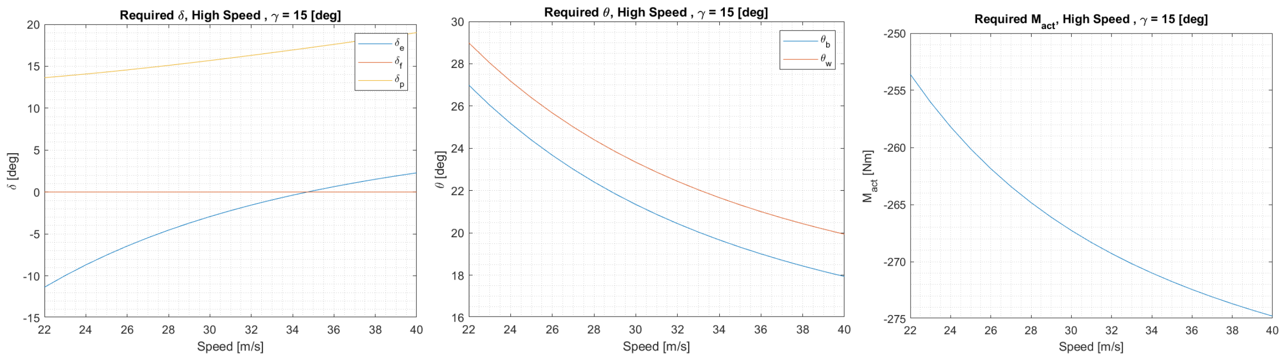

(a) Required δ (b) Required θ (c) Required M_{act}

Figure 3: Trim at high velocity, $\gamma = 15°$.

Figure 4 demonstrates the trimmed values for a descending flight at $\gamma = -15°$ and at high velocity. As expected, the body pitch angle θ_b as well as the required propeller pitch δ_p are lower compared to straight and level flight and climbing at the respective flight velocities. Also here the elevator deflection angle δ_e is not varying much from straight and level flight. The range of velocity where trimming points can be found also remains quite the same like climbing and straight and level flight.

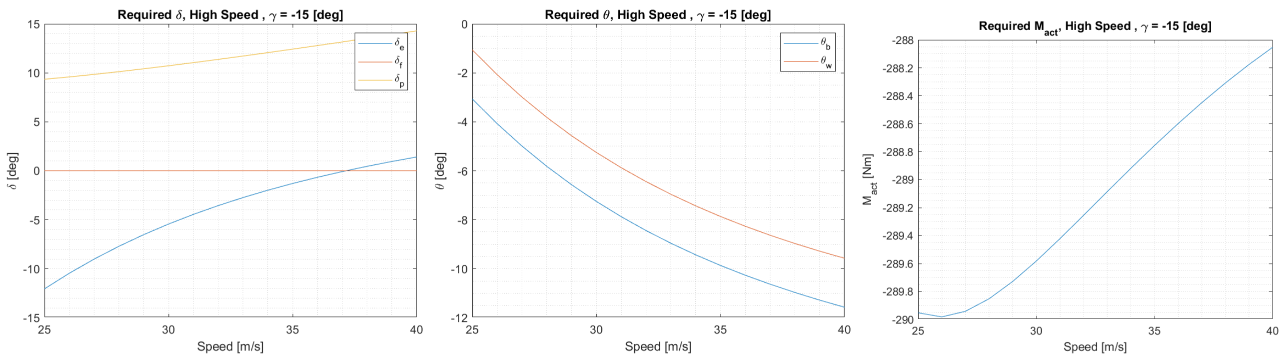

(a) Required δ (b) Required θ (c) Required M_{act}

Figure 4: Trim at high velocity, $\gamma = -15°$.

5.2 Low Velocity Trim

As mentioned in Table 3, for a low-velocity flight the body orientation θ_b and elevator deflection angle δ_e are set to a constant values. The aircraft is controlled by using the wing orientation θ_w, the flaps deflection angle δ_f, and the propeller pitch of the rotors δ_p.

Figure 5 shows that for level flight at $\gamma = 0°$ trim can be found at any velocity lower than 32 [m/s]. However, at a velocity of around 5 [m/s] the graphs are not smooth. The angle of attack in the region of the wing outside the prop-wash is very high (around 90°), causing it to stall. However, the region inside the prop-wash is not stalled. As the velocity increases, the flow from the ambient becomes stronger than the prop-wash stream, resulting in a higher angle of attack and eventually leading to a stall in both regions of the wing: inside and outside the prop-wash. At this point, the wing is not effective and generates mainly drag. Consequently, the wing is tilted back up, and the aircraft behaves more like a multi-rotor. To increase the flight velocity, the wing is tilted down until it is unable to trim using flaps only.

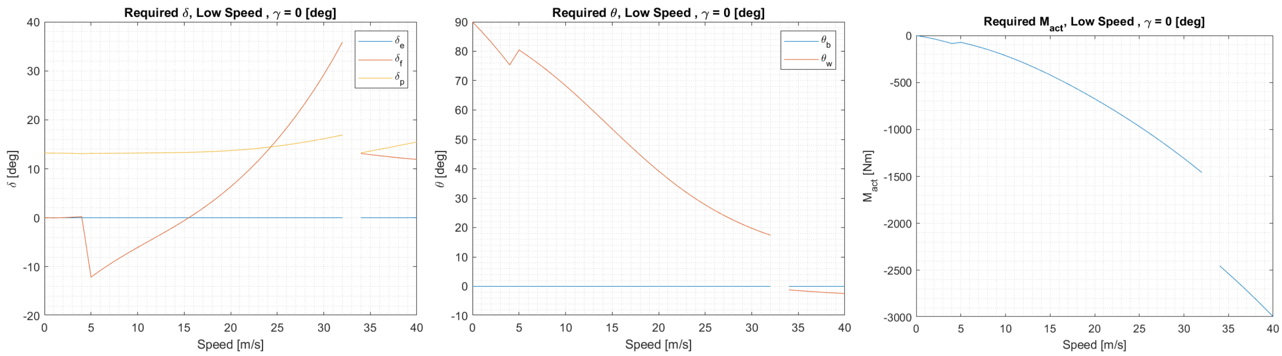

(a) Required δ (b) Required θ (c) Required M_{act}

Figure 5: Trim at high velocity, $\gamma = 0°$.

Figure 6 reveals that trim points for climbing at $\gamma = 15°$ can only be found up to 8 [m/s]. At higher velocities, the flap deflection angle exceeds its limit of 60°. In this case, the performance is poor, and better working points need to be found. Therefore a higher climbing angle of $\gamma = 25°$ is examined.

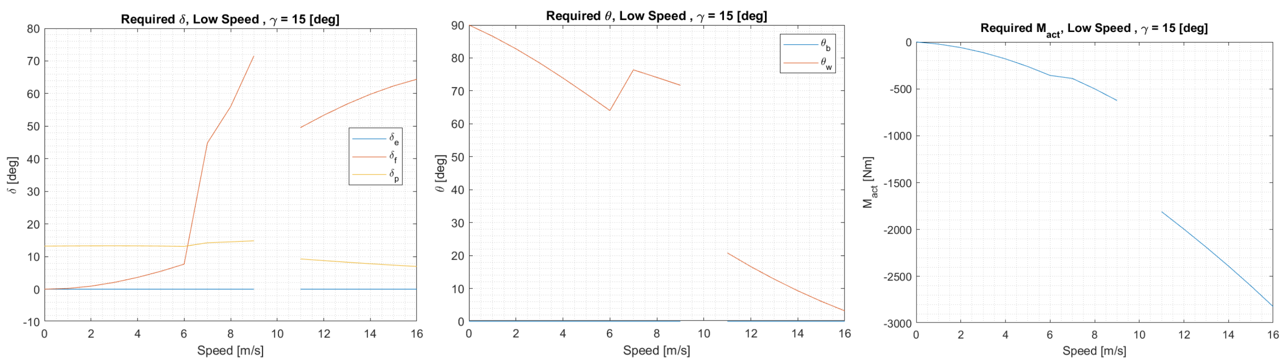

(a) Required δ (b) Required θ (c) Required M_{act}

Figure 6: Trim at high velocity, $\gamma = 15°$.

Figure 7 shows that at a higher climbing angle of $\gamma = 25°$, the flap deflection angle is lower at low velocities, and the required actuator moment remains quite the same. Also, the graphs are smooth at the velocity up to 10 [m/s], indicating that there is no stall of the wing outside the prop-wash at this climbing angle. The required power, which is proportional to the propeller pitch angle δ_p, decreases as the velocity increases, meaning that the wing becomes effective and generates lift at higher velocities.

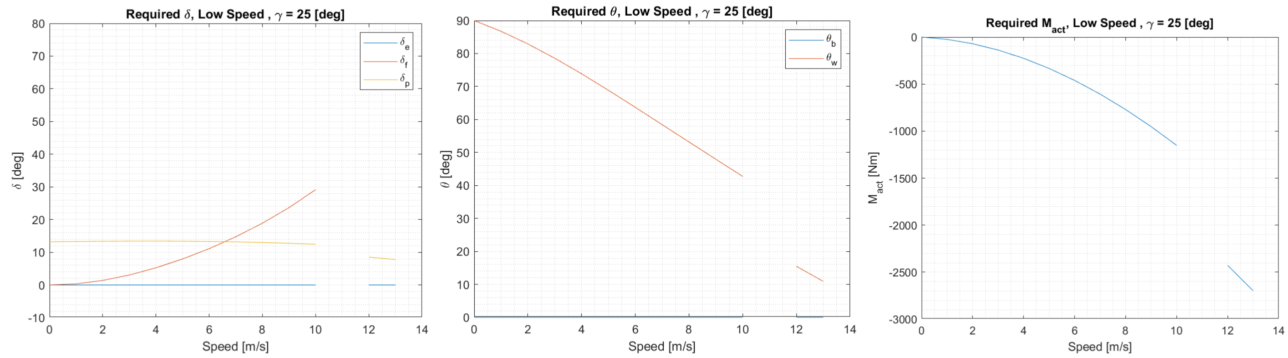

(a) Required δ (b) Required θ (c) Required M_{act}

Figure 7: Trim at high velocity, $\gamma = 25°$.

It might be interesting to examine climbing close to vertical. As demonstrated in Fig. 8, at $\gamma = 85°$, it is possible to trim the aircraft at any velocity, and the wing doesn't stall at any point. This working point will likely be used for the beginning of takeoff. The propeller pitch angle, which is proportional to the required power, increases as the velocity increases, as expected. In this situation, the maximal power of the motor and the maximal propeller pitch angle will limit the maximal flight velocity.

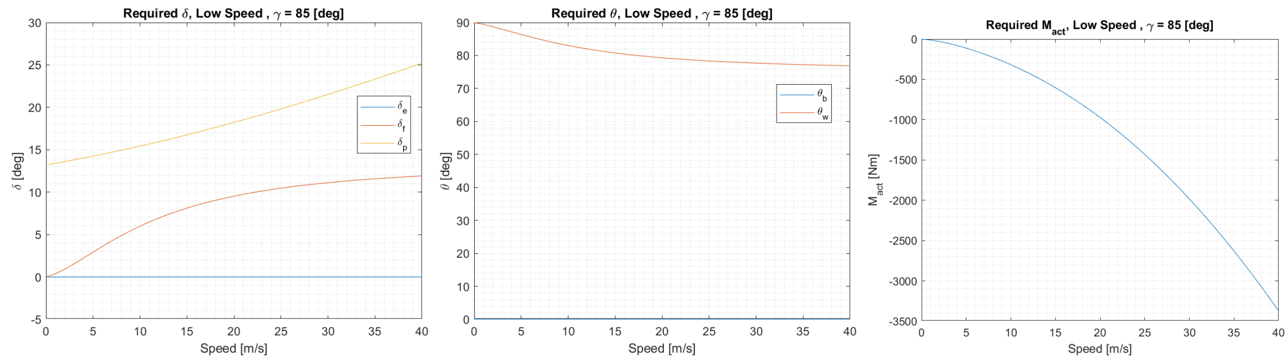

(a) Required δ (b) Required θ (c) Required M_{act}

Figure 8: Trim at high velocity, $\gamma = 85°$.

Demonstrated in Fig. 9, trim points for a descend at $\gamma = -15°$ can be found up to around 5 [m/s]. It can be assumed that the part of the wing inside the prop-wash stalls at 5 [m/s], and it is impossible to trim the aircraft at higher velocity as the flap deflection angle δ_f required for trim exceeds the limit.

Changing the trajectory angle to $\gamma = -25°$, the elevator deflection angle to $\delta_e = -20°$ and the body orientation angle to $\theta_b = -10°$ improves the situation, as demonstrated in Fig. 10. In this case, it is possible to find trim points at any velocity lower than 27 [m/s], after which the flap deflection angle reaches its limit.

It is interesting to examine also if it is possible to descend close to vertical. As shown in Fig. 11, it is possible to trim the aircraft while descending at $\gamma = -85°$ at any velocity lower than 11 [m/s]. This proves that it is possible to land the aircraft almost vertically, reaching a point where the advance velocity u is nearly 0.

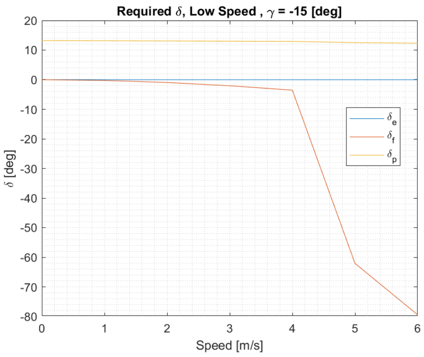

(a) Required δ

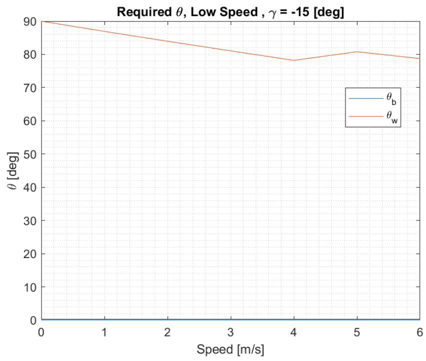

(b) Required θ

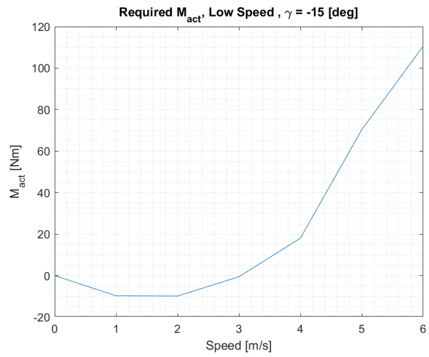

(c) Required M_{act}

Figure 9: Trim at high velocity, $\gamma = -15°$.

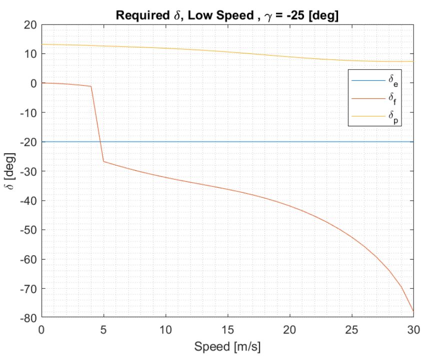

(a) Required δ

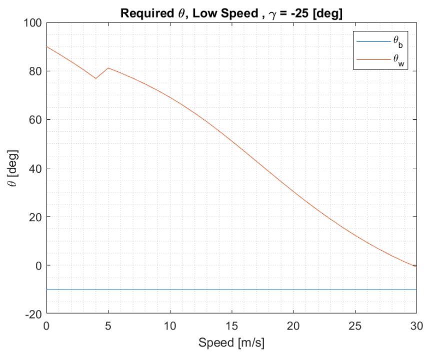

(b) Required θ

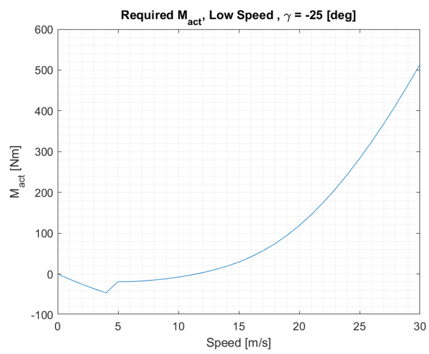

(c) Required M_{act}

Figure 10: Trim at high velocity, $\gamma = -25°$.

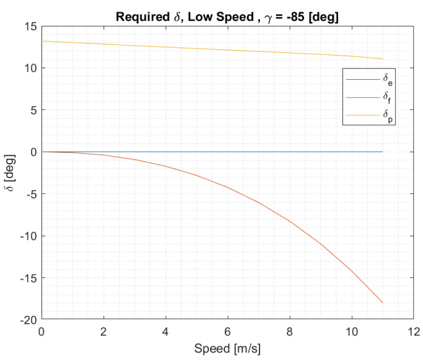

(a) Required δ

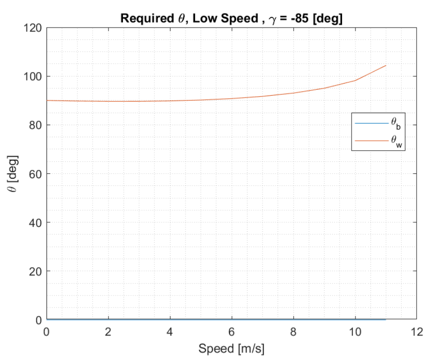

(b) Required θ

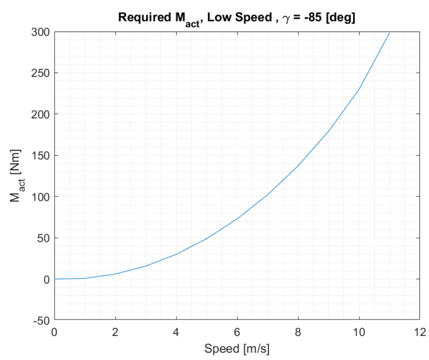

(c) Required M_{act}

Figure 11: Trim at high velocity, $\gamma = -85°$.

6 Center of Gravity

Setting the body's center of gravity far from the hinge (forward or backward) leads to a situation where it is impossible to trim the aircraft when the advance speed is low. It is important to find an analytical expression for this body's center of gravity limit and understand the phenomenon that sets it.

When trimming the aircraft where $u \approx w \approx 0$, forces and moments are mainly produced by the motors and by the wing and flaps in prop-wash wing regions, as in all other regions the dynamic pressure is $q_D \approx 0$. This means that on the aircraft's body, all external forces and moments are produced by the hinge and gravity. Solving (1a) yields $R_x = 0$, and solving (1b) yields $R_z = -m_b g$. Substituting these results into (1c) yields

$$M_{act} = m_b g l_b \cos\theta_b. \tag{6}$$

The wing needs to be trimmed as well for hovering. Solving (2a) and substituting $R_x = 0$ results in $X_w = 0$, while solving (2b) and substituting $R_z = -m_b g$ results in $Z_w = -(m_w + m_b)g$. Substituting these results into (2c) yields

$$M_w = m_b g l_b \cos\theta_b + m_w g l_w \cos\theta_w. \tag{7}$$

As shown in section 5, for trimmed hovering $\theta_w = 90°$. In addition, it will be comfortable to hover when the body attitude angle $\theta_b \approx 0$. Substituting into (7) and isolating l_b we get

$$l_b = \frac{M_w}{m_b g}, \tag{8}$$

meaning that the maximal aerodynamic moment that can be produced by the wing while hovering limits the center of gravity location of the body. Choosing $\omega_p = 1800$ [RPM], and $\delta_p = 13.2°$ the moment generated by the wing as a function of advance velocity for various flap deflection angles δ_f is shown in Fig. 12. It can be inferred that the maximal moment generated by the wing drastically decreases once the wing stalls.

Taking the maximal generated moment when the wing is stalled and substituting it into (8) sets the limit to the body center of gravity

$$l_{b_{max}} \leq \frac{M_{w_{max}}}{m_b g} \approx \frac{154}{450 \cdot 9.81} \approx 3.5 \text{ [cm]} \tag{9}$$

This result may vary when maneuvering or in non-trimmed flight. One of the challenges that must be dealt with is finding trajectories to accelerate from low velocity to high velocity without stalling, and vice versa. This will give the option to develop higher aerodynamic moment on the wing, leading to higher $l_{b_{max}}$.

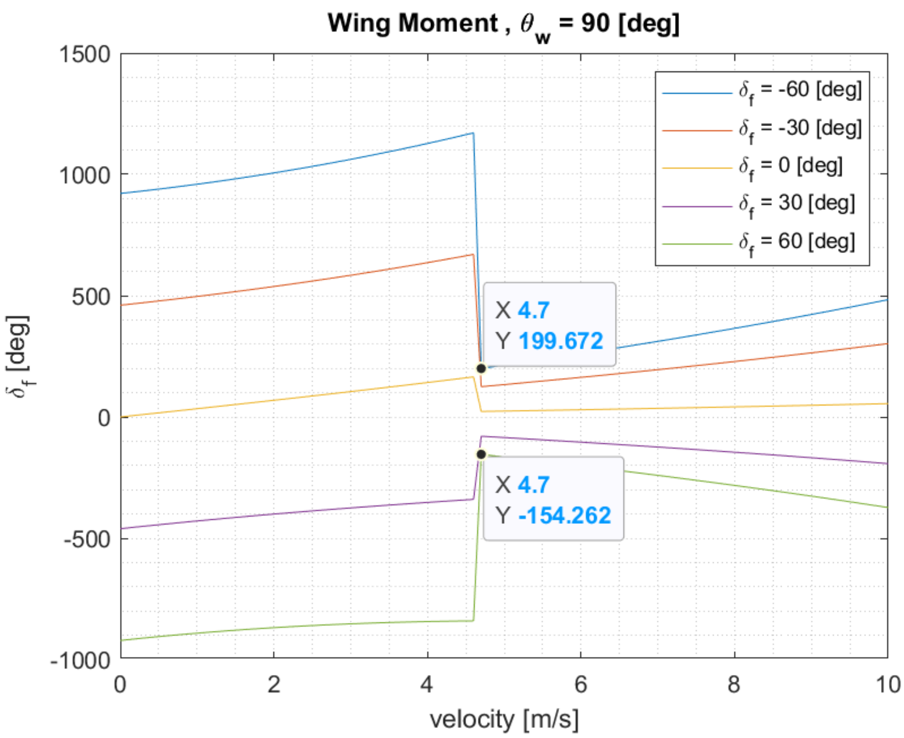

Figure 12: Wing aerodynamic moment around the hinge, $\theta_w = 90°$.

7 Summary

This research focuses on the longitudinal dynamics of a new aircraft configuration. The objective was to determine if it is feasible for the aircraft to take off and land from a specific point. Dynamic and aerodynamic models were developed for the aircraft in the longitudinal plane. The impact of the body center of gravity on the models was tested. The trimming problem was also addressed using the `fsolve` numeric solver in MATLAB. Various flight conditions were tested, including high-velocity flight resembling conventional fixed-wing aircraft, straight and level flight, climbing at a $\gamma = 15°$ angle, and descending at a $\gamma = -15°$ angle were examined. Additionally, low-velocity flight with tilted wings and flaps for control was tested. Straight and level flight, climbing at $\gamma = 15, 25, 85°$ angles, and descending at $\gamma = -15, -25, -85°$ angles were analyzed. It was discovered that setting the elevator at $-20°$ while descending at a $\gamma = -25°$ angle improved performance, and trim could be achieved at any velocity below 27 [m/s].

The next stage of the project will focus on linearization and stability of the model, potentially including time simulation. It will also explore possible and optimized trajectories for takeoff and landing at a specific point, serving as a foundation for designing the aircraft's control system.